Alice C. Quillen
Department of Physics and Astronomy,
University of Rochester,
Rochester, NY 14627
e-mail: alice.quillen@rochester.edu

Randal C. Nelson
Department of Computer Science,
University of Rochester,
Rochester, NY 14627
e-mail: nelson@cs.rochester.edu

Hesam Askari
Department of Mechanical Engineering,
University of Rochester,
Rochester, NY 14627
e-mail: askari@rochester.edu

Kathryn Chotkowski
Department of Physics and Astronomy,
University of Rochester,
Rochester, NY 14627
e-mail: kchotkow@u.rochester.edu

Esteban Wright
Department of Physics and Astronomy,
University of Rochester,
Rochester, NY 14627
e-mail: ewrig15@ur.rochester.edu

Jessica K. Shang
Department of Mechanical Engineering,
University of Rochester,
Rochester, NY 14627
e-mail: j.k.shang@rochester.edu

A Light-Weight Vibrational Motor Powered Recoil Robot That Hops Rapidly Across Granular Media

A 1-cm coin vibrational motor fixed to the center of a 4-cm square foam platform moves rapidly across granular media at a speed of up to 30 cm/s or about 5 body lengths/s. Fast speeds are achieved with dimensionless acceleration number, similar to a Froude number, up to 50, allowing the light-weight 1.4 g mechanism to remain above the substrate, levitated and propelled by its kicks off the surface. The mechanism is low cost and moves across granular media without any external moving parts. With 2-s exposure, we photograph the trajectory of the mechanism with an LED fixed to the mechanism. Trajectories can exhibit period doubling phenomena similar to a ball bouncing on a vibrating table top. A two-dimensional robophysics model is developed to predict mechanism trajectories. We find that a vertical drag force is required in the model to match the height above the surface reached by the mechanism. We attribute the vertical drag force to suction from air flow below the mechanism base and through the granular substrate. Our numerical model suggests that horizontal speed is maximized when the mechanism is prevented from jumping high off the surface. In this way, the mechanism resembles a galloping or jumping animal whose body remains nearly at the same height above the ground during its gait. Our mechanism and model illustrate that speed and efficiency of light-weight hoppers on granular media can be affected by aerodynamics and substrate permeability.
[DOI: 10.1115/1.4044333]

Keywords: dynamics, microscale mechanisms and robotics, theoretical kinematics

1 Introduction

Limbless locomotion by snakes or worms gives a paradigm for locomotion in rough and complex environments [1–5]. Soft and hard robotic devices can crawl over a surface due to an asymmetric or directional dynamic friction (e.g., Refs. [6–9]). Snakes and snake-like robots (e.g., Refs. [10–12]) propel themselves by exploiting asymmetry in the friction they generate on a substrate.

Vibrating legged robots provide a different, but a related example of locomotion that also exploits frictional asymmetry (e.g., Refs. [13,14]). These are the mechanisms of minimal complexity that exploit periodic shape changes to propel themselves (e.g., Refs. [7–9,15]). Modulation of friction due to oscillations of the normal forces causes stick-slip horizontal motions and net horizontal displacement. An example is the table top bristlebot toy that can be constructed by fixing a low-cost vibrational motor to the head of a toothbrush [16]. Examples of vibrationally powered mechanisms include miniature robots (e.g., Refs. [17–19]) that are smaller than a few centimeters in length.

The granular medium presents additional challenges for a locomotor (e.g., Ref. [10]) as propelled grains or particles can jam the mechanism and exert both drag-like and hydrostatic-like forces [20–22]. A vibrating mechanism can sink into the medium causing mechanism to tilt or impeding its motion, or the mechanism may float due to the Brazil nut effect (e.g., Ref. [23]). A variety of animals propel themselves rapidly across granular surfaces. The light-weight zebra-tailed lizard (10 cm long, 10g) moves 10 body lengths/s [24]. The six-legged DynaRoACH robot (10 cm, 25 g) is a rotary walker that approaches a similar speed (5 body lengths/s) on the granular media [25].

In this paper, we work in the intersection of these fields, exploring how light-weight, small, vibrating, and legless locomotors, a few centimeters in size, can move rapidly on the surfaces of the granular media. An advantage of a legless locomotor is that appendages cannot get jammed or caught in the mechanism. As most small animals that traverse sand either use legs or wiggle, our locomotors have no direct biological counterparts but they are similar to vibrating table top toys. They are in a class of mechanisms that locomote due to recoil from internal motions (e.g., Ref. [26]). Small vibrational motors are low cost, so if autonomous locomotors can be devised with them, large numbers of them could be simultaneously deployed for distributed exploration.

In this manuscript, we describe, in Sec. 2, the construction of a light-weight (less than 2 g) and low-cost mechanism (a few dollars) that can traverse granular media at a speed of a few body lengths per second. We estimate an acceleration parameter or Froude number for the mechanism, classifying it as a jumper or hopper, in comparison to animal gaits. Because the mechanism trajectories often show the mechanism touching the substrate once per motor oscillation and with gravitational forces alone they should remain airborne longer, we infer that there must be a force pulling the mechanism downward. In Sec. 3, we estimate that airflow through the granular medium could affect the mechanism motion. Measurements of the air flow rate as a function of pressure are used to estimate the size of this suction force in Sec. 3.2. In Sec. 4, we develop a

Contributed by the Mechanisms and Robotics Committee of ASME for publication in the Journal of Mechanisms and Robotics. Manuscript received July 31, 2018; final manuscript received June 27, 2019; published online July 25, 2019. Assoc. Editor: Robert J. Wood.

two-dimensional model for the mechanism motion that takes into account pressure due to airflow. A comparison between our robophysical model and our mechanism trajectories illustrates that aerodynamics and substrate permeability can affect the dynamics and design of light-weight locomotors on complex media.

2 Mechanism Construction and Experimental Setup

We place a 5 V DC coin vibrational motor on a light rigid foam platform (see Fig. 1). The motor is 1 cm in diameter and rotates at approximately 12,000 rpm. The foam platform is rectangular and a few centimeters long but only a few millimeters thick. The foam is a closed-cell, moisture-resistant rigid foam board, composed of extruded polystyrene insulation (XPS) made by Owens Corning. Its density is 1.3 pounds per cubic foot which is 0.0208 g/cm^3. The coin vibrational motor is oriented, so a flat face is perpendicular to the foam board. To rigidly fix the motor to the foam board platform, we used a double-sided tape attached on either side of the motor and to small foam blocks that are also attached to the platform, as shown in Fig. 1. The motor is externally powered with a DC power supply and via light and ultra-flexible wire so as not to interfere with locomotion. The wire we used is a thin and flexible multi-strand silver-plated copper 36AWG wire with silicone rubber insulation.

Inside the vibrational motor is a lopsided flywheel, giving a displacement between the center of mass of the motor and its case. When the motor rotates, recoil from the flywheel causes the motor case to vibrate back and forth and up and down. In the absence of external forces, and if prevented from rotating, the motor case moves in a circle, as illustrated in Fig. 2. The motor is designed to rotate at 12,000 rpm (200 Hz) at 5 V DC. However, we have found that the frequency depends on DC voltage, ranging from $f \approx 180$–280 Hz over a voltage range of 3.5–5.5 V.

When the mechanism is light, the recoil from the lopsided internal flywheel inside the motor causes the entire mechanism to jump off the surface. If the horizontal component of the recoil is non-zero

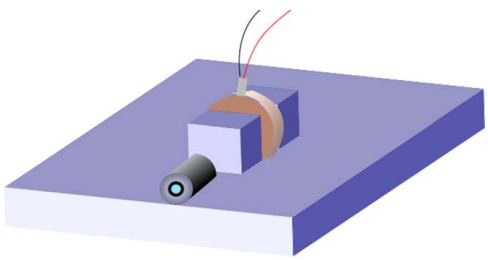

Fig. 1 An illustration of the hopper mechanism. A 1-cm diameter coin vibrational motor is fixed to a 4 × 4 × 0.5 cm foam platform. An LED is used to track its motion. The LED is covered with foil tape that has been punctured with a pinhole. Wires and a resistor for the LED are not shown.

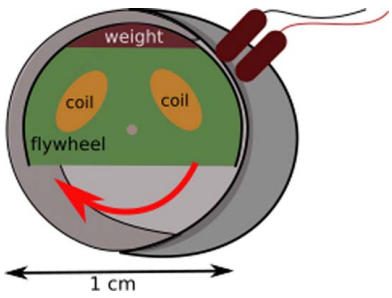

Fig. 2 An illustration of the inside of a coin vibrational motor. The motor case is rigid. A lopsided flywheel inside rotates causing the entire case to move in a circle in a direction countering the motion of the internal weight.

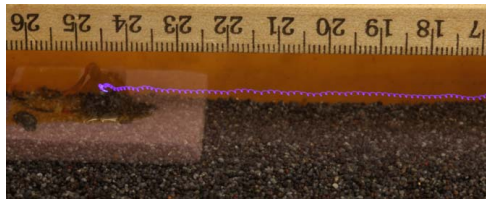

Fig. 3 Photograph showing a 2-s exposure in ambient room lighting. The exposure was started when the mechanism was stationary and on the left. Then, the motor was turned on, and the mechanism moved to the right. A blue LED is mounted on the mechanism. The bouncing trajectory of the mechanism is traced by the moving position of the LED, giving a series of loops as the mechanism hops to the right. We measure the speed of the mechanism by counting the loops, using the frequency of the motor and distances measured with the ruler mounted above the mechanism. Mechanism displacement, *A*, caused by motor recoil is estimated from the vertical amplitude of the trajectory loops. The substrate in this photograph is black poppy seeds, and the motor frequency is 220 Hz.

when the mechanism lands, friction between surface and mechanism base propels the mechanism horizontally. The recoil from the flywheel lets the mechanism propel itself when it kicks itself off the surface.

To track mechanism motion, we attached a small clear blue LED to the platform. The LED is powered in series with a 100-Ω resistor. The LED is covered with the foil tape that has been punctured by a pinhole and is powered with the same DC power lines as used to power the motor. The mechanism weight totaled 1.4 g.

Our experimental setup is shown in Fig. 3. The mechanism is placed on a flat granular bed. The grains are poppy seeds, cornmeal, or millet; however, we have also tested our mechanisms on dry sand and coarse table salt. Dry agricultural grains have been used as granular substrates in previous robophysical studies (e.g., Ref. [22]) and were adopted here because the grains are fairly uniform in shape and size. We do not press or compactify the granular media but do sweep it flat prior to taking photographs. Granular materials can be described by an angle of repose θ_{repose}. By tilting the trays holding the media, we measured $\theta_{\text{repose}} \approx 34$ deg for the granular materials discussed here: poppy seeds, cornmeal, and millet. The angle of repose is related to the coefficient of static friction μ_s with $\tan\theta_{\text{repose}} = \mu_s$. For our granular materials, the coefficient of static friction $\mu_s \sim 0.7$ and is similar to that of sand used in playgrounds and that of coarse table salt.

A camera with a macrolens was used to photograph the mechanism in motion. We open the camera shutter and then turn on the motor. With a 2-s exposure, the motion of the mechanism is tracked with the light from the LED, as shown in Fig. 3. With the room lights on, we can see the original location of the mechanism and the LED track as the mechanism moved to the right. Subsequent photographs, shown in Figs. 4 and 5, were taken in the dark and show only the tracks made by the LED. A ruler mounted above the mechanism (see Fig. 3) gives the scale in centimeters. We have also filmed the motion of the mechanism with a high-speed camera at 1000 frames per second.[1]

We took audio recordings of the mechanism while in motion. We measured the dominant frequency present in the sound files and this gave a measurement for the vibrational motor frequency. This way we could determine the frequency of vibration at different DC voltages and for specific mechanisms. For the trajectories shown in Fig. 4, the audio recorded motor frequencies were 175, 220, and 285 Hz at 3, 4, and 5.5 V, respectively. With the motor frequency, and by counting the number of loops per centimeter in the LED trajectory, we can compute the speed of the mechanism as it traverses the granular medium. Figure 4 shows three pairs of photographs

[1] https://youtu.be/kLsG6e_-IqM

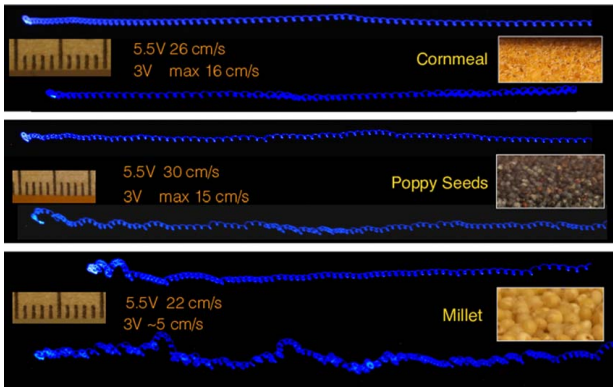

Fig. 4 Mechanism trajectories on three different substrates and at two different motor voltages. The curly lines show the tracks of the blue LED during 2-s exposures. The top pair of trajectories show the mechanism on cornmeal, the middle pair on poppy seeds, and the bottom pair on millet. Subpanels on the left show a 1-cm scale and views of the granular substrate on the right. The subpanels were extracted from the setup photographs without rescaling them. At 3 V, the motor frequency was 175 Hz, whereas at 5.5 V, it was 285 Hz.

Fig. 5 A photographed trajectory illustrating period doubling and tripling. This is a trajectory of a somewhat more massive mechanism (1.7 g) with a larger displacement ($A \sim 0.5$ mm), a frequency of 240 Hz and on cornmeal.

showing the mechanism moving across three different substrates: cornmeal, poppy seeds, and millet. On each substrate, we set the motor voltage to 3 V or 5.5 V. The lower trajectory in each pair shows the lower voltage setting. Measured horizontal speeds are labeled as text on Fig. 4 for each trajectory. For each experiment, we took a photograph of the experimental setup with the same camera setup and focus. An extracted region of the ruler from the setup photographs gives a scale and are shown in the subpanels in Fig. 4. From the same setup photographs, we also cut out subpanels showing the granular media.

Mechanism trajectories seen in Figs. 3 and 4 exhibit regions of periodic behavior. During these times, the mechanism touches the substrate once per motor oscillation period. Period doubling describes when the mechanism touches down once for every two oscillation periods. Figure 4 also shows regions where period doubling occurs; for example, see the lower trajectory on cornmeal. Figure 5 shows a trajectory from a heavier mechanism and a motor giving a larger displacement at 240 Hz on cornmeal that illustrated period doubling and tripling.

To measure the motor recoil, we filmed a bare vibrational motor hanging from a thread. Horizontal peak to peak motions were about 1 mm giving an amplitude of vibrational motion of about $A_{\text{bare}} \sim 0.5$ mm. The motor itself weighs only $m_{\text{motor}} \sim 0.9$ g, whereas the entire mechanism is more massive, $M \sim 1.4$ g. With the motor affixed to the platform, the amplitude of motion for the entire mechanism (in free space) depends on the ratio of the mass of bare motor m_{motor} to mass of mechanism M, $A \sim A_{\text{bare}}(m_{\text{motor}})/M \sim 0.3$ mm.

We can also estimate the recoil amplitude from our photographs. Amplitude $A \sim 0.3$ mm is consistent with the vertical length of the loops in the trajectories of Fig. 4. At a fixed voltage, we compared the frequency, measured from audio recordings, of a bare motor hanging from a thread to one affixed to a mechanism that is moving across a granular substrate. The two frequencies are similar, so the locomotion does not significantly slow down or load the motor.

When turned on, a bare vibrational motor sitting on the surface of a granular medium digs a small crater and remains vibrating in the bottom of it, rather than moving across the surface. The foam platform of our mechanism distributes the force on the granular substrate associated with the motor motion. For these mechanisms, the granular medium is barely disturbed as the mechanism moves across it. Only on cornmeal is a faint track left behind as the mechanism moves across it. On millet and poppy seeds, before and after photographs showed that only a few grains were disturbed after the mechanism traversed the surface. Granular media is often described in terms of a flow threshold or critical yield stress [27]. At stresses below the critical one, grains do not move. Our hopper mechanism exerts such low stress on the granular medium that the critical yield stress of the granular medium is not exceeded. There are trade-offs in choosing the surface area and thickness of the foam platform. If the mechanism is too heavy, it will not jump off the surface and its speed is reduced. If the platform is too small, then the vibrating mechanism craters (digs in) instead of moving across the surface. If the platform is too thin, it flexes and this can prevent locomotion if the corners vibrate and dig into the medium. Smaller platforms are less stable as irregularities in the substrate can tip them. The fastest mechanisms have stiff platforms and motors mounted low and centered on the platform.

The acceleration of the mechanism base

$$A\omega^2 = 475\,\text{m}\,\text{s}^{-2}\left(\frac{A}{0.3\,\text{mm}}\right)\left(\frac{12{,}000\,\text{rpm}}{f}\right)^2 \tag{1}$$

where $\omega = f/(2\pi)$ is the angular frequency of vibration. The vibration causes the mechanism to move with velocity,

$$A\omega = 38\,\text{cm}\,\text{s}^{-1}\left(\frac{A}{0.3\,\text{mm}}\right)\left(\frac{12{,}000\,\text{rpm}}{f}\right) \tag{2}$$

This is a maximum velocity for the mechanism's horizontal motion. The horizontal velocities reached by our mechanisms can be up to 0.6 times this maximum.

2.1 Acceleration Parameter or Gait Froude Number. We estimate the time it takes the mechanism to fall the distance of the vibration or displacement amplitude $t_g = \sqrt{A/g}$, where g is the acceleration due to gravity. We can derive a dimensionless quantity by comparing this time to the vibration angular frequency $t_g\omega = \sqrt{A/g}\omega$. The ratio of the acceleration due to vibrational oscillation $A\omega^2$ and that due to gravity g is

$$\Gamma = \mathbf{Fr} \equiv \frac{\omega^2 A}{g} \tag{3}$$

and this is equivalent to $(t_g\omega)^2$. This dimensionless number is also the ratio of centripetal force to gravity force and is also known as a walking or gait Froude number. Gait frequency for animals scale with Froude number [28], with a walker having $\mathbf{Fr} \lesssim 1$.

The dimensionless ratio Γ is equivalent to an acceleration parameter used to classify the dynamical behavior of a hard elastic object bouncing on a vibrating plate but computed using the displacement and frequency of the table rather than the mechanism (e.g., Refs. [29–32]). Using the amplitude of motion and motor frequency of 280 Hz, we estimate an acceleration parameter for our mechanism of about $\Gamma \sim 48$. As $\Gamma \gg 1$, our mechanism can be considered as a hopper or a galloper rather than a walker. Gaits in animals depend on Froude number with the transition to galloping taking place at about $\mathbf{Fr} \sim 4$ [28,33].

Our mechanism can launch itself off the surface with a velocity $v_0 = A\omega$ so the mechanism base should reach a maximum height above the substrate of

$$h_{\max} = \frac{v_0^2}{2g} = \frac{\Gamma A}{2} \tag{4}$$

It should remain airborne for a time

$$t_{\text{airborne}} = \frac{2A\omega}{g} = \frac{2\Gamma}{\omega} = \frac{\Gamma}{\pi} P_{\text{osc}} \tag{5}$$

with $P_{\text{osc}} = 2\pi/\omega$ the oscillation period. The acceleration parameter sets the maximum height reached by the mechanism base. For an acceleration parameter of about 36 (for the 3 V trajectories in Fig. 4), the height reached by the mechanism should be $h_{\max} = 15A$ and it should remain airborne for about 9 oscillation periods. The maximum height reached during a long jump by the mechanism is approximately equal to $A\Gamma/2$ (for $A \sim 0.3$ mm, $\Gamma \sim 36$, $h_{\max} \sim 5$ mm) and that is consistent with the maximum heights sometimes reached in the 3 V trajectories shown in Fig. 4. However, the photographed trajectories show that most of time, the mechanism touches the surface once per motor oscillation period and remains within 2 $A \sim 0.6$ mm from the surface. The discrepancy between maximum height predicted from the acceleration parameter and that observed is about an order of magnitude. There must be an additional force preventing the mechanism from leaving the surface at a velocity $A\omega$. If the medium allowed the mechanism to bounce elastically, then the maximum height could be even higher. Friction cannot pull the mechanism downward, and a downward force is needed to keep the mechanism from reaching larger heights than we have observed.

We consider additional forces that could reduce the mechanism's upward vertical velocity and jump height. We filmed the mechanism moving across poppy seeds with a high-speed video camera at 1000 frames per second (fps). In the high-speed videos, we did not see the platform rock or flex much, though waves excited by vibration can propagate down the power wires. It is unlikely that these two types of motion could consistently pull the mechanism downward as stiffer mechanisms with a polystyrene platform base behaved similarly to those with softer platform bases made of polyethylene foam. This led us to consider the role of aerodynamics. We found that a mechanism with a flat platform base on a very flat surface (a glass sheet) horizontally moved slowly, but after we poked holes in the platform, its speed across the surface was increased. A mechanism constructed with a soft polyethylene base moved more slowly after it had traversed a rough carpet that abraded its base. We found that a mechanism on a solid plate containing holes jumped higher and more irregularly than when moving on a granular surface or a solid flat plate. A mechanism under vacuum (1/100th of an atmosphere) moved more irregularly than the same mechanism under the atmospheric pressure. A mechanism moving over a granular medium covered in a light powder (cornstarch) blew the powder an inch away from the mechanism. These experiments imply that the air flow beneath the mechanism affects its motion.

3 Aerodynamics

We estimate the pressure that would develop under the platform using Bernoulli's principle. We estimate the pressure with $\rho_{\text{air}} u_{\text{air}}^2$, where ρ_{air} is the density of air and u_{air} is the horizontal velocity of air under the mechanism platform. Placing the pressure in units of acceleration on the mechanism, we estimate an acceleration on the mechanism $a_B \sim (\rho_{air} u_{air}^2 L^2)/M$, where L^2 is the surface area of the mechanism platform base. In units of the acceleration $A\omega^2$, the acceleration estimated with Bernoulli's principle

$$\begin{aligned}\frac{a_B}{A\omega^2} &\approx \left(\frac{u_{\text{air}}}{A\omega}\right)^2 \frac{\rho_{air} A L^2}{M} \\ &\approx 0.007 \left(\frac{u_{\text{air}}}{A\omega}\right)^2 \left(\frac{L}{4\text{ cm}}\right)^2 \left(\frac{\rho_{\text{air}}}{1.2 \times 10^{-3}\text{ g/cc}}\right) \\ &\quad \times \left(\frac{1.4\text{ g}}{M}\right)\left(\frac{A}{0.3\text{ mm}}\right)\end{aligned} \tag{6}$$

The ratio is low, suggesting that aerodynamics cannot affect the mechanism dynamics. However, we reconsider this conclusion when we take into account airflow when the mechanism is nearly touching the substrate.

When the height is low and the mechanism about to land, the horizontal air velocity below the mechanism should exceed the vertical mechanism velocity. We relate the volume flow rate of air between mechanism and substrate to the vertical velocity of the mechanism platform v_z, the platform's surface area, and z its height above the substrate:

$$\frac{dV}{dt} \approx 4Lzu_{\text{air}} = L^2 v_z \tag{7}$$

This gives a speed

$$\frac{u_{\text{air}}}{A\omega} \approx \frac{L}{4z}\frac{v_z}{A\omega} \approx 30\left(\frac{L}{4\text{ cm}}\right)\left(\frac{A}{z}\right)\left(\frac{0.3\text{ mm}}{A}\right)\left(\frac{v_z}{A\omega}\right) \tag{8}$$

If we insert this into Eq. (6), we find that the estimated pressure force would be significant when the platform is quite near the surface $z \sim A$, and in that setting, we should consider flow through the narrow space between platform and substrate and through the substrate itself.

In narrow spaces, air viscosity can be important. The kinematic viscosity of air ν_{air} in units of the acceleration parameter $A^2\omega$ is not that small,

$$\frac{\nu_{\text{air}}}{A^2\omega} \approx 0.1\left(\frac{\nu_{\text{air}}}{0.15\text{ cm}^2\text{ s}^{-1}}\right)\left(\frac{0.3\text{ mm}}{A}\right)^2\left(\frac{1257\text{ s}^{-1}}{\omega}\right) \tag{9}$$

As our grain sizes are similar to the mechanism vibrational amplitude A, air motions close to or in between grains can be in the low Reynolds number regime.

We consider the mechanism at rest after landing on the substrate. When the mechanism is pushing off the surface, the air speed between grains would be low. Because the Reynolds number is proportional to speed, the Reynolds number could be low and so air viscosity could be important. Because of irregularity in the surface, we can consider the gaps between the mechanism platform and the granular medium as a permeable medium that air must flow through (see Fig. 6 for an illustration).

In a permeable or porous medium, Darcy's law relates the flow velocity $\mathbf{u}$ in a fluid to the pressure gradient ∇p

$$\mathbf{u} = -\frac{\kappa}{\mu}\nabla p \tag{10}$$

with $\mu = \nu\rho$ the dynamic viscosity and κ the porous medium's permeability. Permeability has units of area and depends on the interstitial spaces. An air pressure gradient is required for air to flow beneath the mechanism base. For air to flow under the mechanism, the pressure must be lower under it than outside it. This causes a suction on the mechanism. As the air flow velocity $u \propto v_z$ is approximately proportional to the vertical velocity of the platform, Eq. (10) suggests that the force on the mechanism (or pressure per unit area)

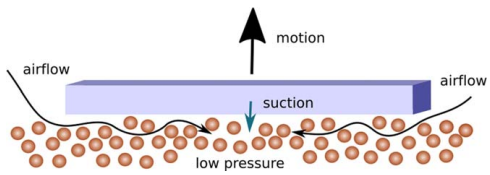

Fig. 6 For the mechanism to launch itself off the substrate, air must flow beneath its platform base. The air pressure under the platform must be lower than the ambient pressure for the air to flow under the mechanism platform. The lower pressure exerts suction on the platform base. The permeability of the space between platform and substrate and of the granular substrate affects mechanism locomotion.

due to air pressure is proportional to v_z. This gives a damping force on the mechanism that is important only when the mechanism is touching or nearly touching the granular medium. Air suction can pull the mechanism down so it could explain why the mechanism did not reach the height we estimated from the acceleration parameter in Sec. 2.1.

3.1 Half-Space Flow Field in a Permeable Medium. To estimate the size of a force due to air pressure on the mechanism base, we consider a circular platform with radius $r_h = L/2$ on a permeable medium. We describe the air pressure and flow velocity in the permeable medium in cylindrical coordinates r, z and assuming azimuthal symmetry. Here, $z<0$ below the granular substrate, $z=0$ on the surface, and the origin is in the center of the platform that is touching the granular medium but at the moment it lands or takes off vertically from the surface. The air pressure on the surface is $p(r,\ z=0)$. We take atmospheric pressure to be zero (describing pressure with a difference from atmospheric), so $p(r_h,\ z=0)=0$ on the edge of the platform.

We use Darcy's law (Eq. (10)) to relate air flow velocity $\mathbf{u}$ to the air pressure gradient in the granular medium. Darcy's law combined with the condition for incompressible flow, $\nabla\cdot\mathbf{u}=0$, yields Laplace's equation for pressure $\nabla^2 p=0$. The boundary conditions determine the solution for the pressure $p(r,\ z)$. The flow field is then set by the pressure gradient.

On the half-space with $z<0$, a solution to Laplace's equation in cylindrical coordinates that is well behaved at the origin and large negative z is $p_k(r,\ z)\propto J_0(kr)e^{kz}$, where J_0 is a Bessel function of the first kind. The general solution would be a sum or integral (over k) of such terms. Because the pressure is zero at $r=r_h$, $z=0$, the Bessel function must have a root at $r=r_h$. The first root of $J_0(x)$ is at $x\approx 2.4$. We approximate the pressure profile under the platform with a single Bessel function

$$p(r,\ z)=p_0 J_0(2.4r/r_h)e^{2.4z/r_h} \tag{11}$$

where the peak pressure under the mechanism is p_0.

We take the derivative of this solution with respect to z and use Darcy's equation to estimate the vertical component of the flow velocity

$$u_z(r,\ 0)=-\frac{\kappa}{\mu_{\text{air}}}\frac{dp}{dz}(r,\ z)\bigg|_{z=0}=u_c J_0(2.4r/r_h) \tag{12}$$

with central velocity

$$u_0=-\frac{\kappa}{\mu_{\text{air}}}\frac{2.4}{r_h}p_0 \tag{13}$$

It is convenient to compute $\int_0^{2.4} dx\ xJ_0(x)=1.24$. The average $\bar{u}_z=1/(\pi r_h^2)2\pi\int_0^{r_h} r\ dr\ u_z(r,\ 0)\sim u_0/2$. The pressure integrated over the base area $2\pi\int_0^{r_h} p(r,\ 0)r\ dr\sim 1.4p_0 r_h^2$.

With the platform vertical velocity v_z equal to the average $\bar{u}_z$, we estimate the force on the mechanism from pressure integrated over the area of the platform base and using Eq. (12)

$$\begin{aligned} F_{\text{aero}} &\sim 2\pi\int_0^{r_h} p(r,\ 0)r\ dr\sim 1.4p_0 r_h^2 \\ &\sim -\frac{\mu_{\text{air}}}{\kappa}r_h^3 v_z\sim -\frac{\mu_{\text{air}}}{\kappa}\frac{L^3}{8}v_z \end{aligned} \tag{14}$$

It is convenient to write the velocity-dependent aerodynamic damping force in terms of the acceleration on the mechanism

$$a_{z,\text{aero}}\sim\frac{F_{\text{aero}}}{M}\approx -\alpha_z\omega v_z \tag{15}$$

with α_z a dimensionless parameter,

$$\alpha_z\equiv\frac{\mu_{\text{air}}}{\kappa}\frac{L^3}{8M\omega} \tag{16}$$

In Sec. 3.2, we experimentally estimate the coefficient α_z, giving the force on the mechanism due to air flow through the permeable substrate. In Sec. 3.3, we modify Eq. (15) to take into account the flow between mechanism base and substrate when the mechanism is close to but above the surface and using a Plane Poisseuille flow model for viscous flow between two plates. In Sec. 4, we incorporate our estimates for α_z into numerical models for the mechanism locomotion.

3.2 Air Flow Rate Versus Pressure Measurements. To estimate the coefficient α_z in Eq. (16), which describes the drag force due to air pressure, we experimentally measured how the air flow rate beneath a block and through our granular media depends on air pressure. We adopted a test geometry similar to that of our mechanism by placing a block on the surface of a granular substrate. The block has a flat base that has an annular shape, with an outer diameter of $d_o=6$ cm and an inner hole with a diameter of $d_i=2.5$ cm. The air within the inner hole is placed under pressure, but outside the annular block, the granular medium is open to atmospheric pressure, see Fig. 7 for an illustration of the experiment. A hose supplied air to the inner hole and escaped through the substrate and the gap between the substrate and the lower surface of the block.

Air was supplied to the inner hole at controlled pressure (above atmospheric) using a bubble regulator. Our device supplies air at pressures of 250–2000 Pa and uses water height to measure pressure. Pressure remained within about ±1/4 in of water (±60 Pa) of each set value. We measured the air volume flow rate using a homemade soap-bubble flow meter, where a soap film rises in a graduated transparent tube of constant diameter. Timing the transit times between marks on the tube gave a measure of the volume flow rate of air. For each experiment, we measured the flow rate at about eight different set pressures. During measurements, the annular block was weighted with a 12-oz weight (3.3 N) to prevent the air pressure from lifting the block and distorting the contact. The percentage error in the pressure at 1" H_2O is 25% while the percentage error in the time is only a few percent. At the higher end, the pressure measurement is good to 4%, but the flow rates are only good to 10–15%.

We measured flow rates dV/dt in cc/s for a block spaced 0.1 mm above a glass sheet, on 120-grit sandpaper (115 μm particle sizes), on common table salt (with a mix of grain diameters in the range 0.25–0.5 mm), cornmeal, and millet. Grain diameters for cornmeal and millet are listed in the notes to Table 1. For the experiments above a glass sheet and on sandpaper, the substrates have solid bases, so air is restricted to travel in the narrow space between the block and the glass plate or paper backing on the sandpaper. For these two experiments, we estimate the air flow velocity $u=(dV/dt)(1/a_w)$ in the middle of the block annulus using cross-sectional area $a_w=2\pi w\ (d_o+d_i)/4$. For the block on glass experiment, the spacing between block and glass plate is $w=0.1$ mm. For the block on 120-grit sandpaper experiment, we use a width

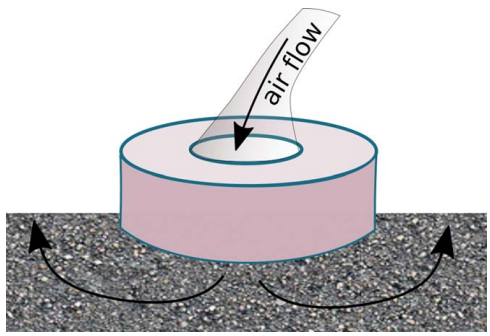

Fig. 7 Flow rate versus pressure measurements were taken for air forced under a flat annular block from its central hole while it was resting on a granular substrate

Table 1 Approximate quantities

f	Vibrational motor frequency	200 Hz (12,000 rpm)
ω	Motor angular frequency	1257 s^{-1}
m_{motor}	Mass of vibrational motor	0.9 g
M	Mass of mechanism	1.4 g
L	Dimension of platform	4 cm
A	Amplitude of motion (whole mechanism)	0.3 mm
$2A_{bare}$	Displacement of bare motor (peak to peak)	1.0 mm
$A\omega$	Velocity of vibration	38 cm/s
$A\omega^2$	Acceleration of vibration	475 m s^{-2}
g	Gravitational acceleration	9.8 m/s^2
ρ_g	Density of granular medium	1 g/cc
μ_s	Coefficient of static friction	≈0.7
ρ_{air}	Density of air	1.2×10^{-3} g/cc
ν_{air}	Kinematic viscosity of air	1.5×10^{-5} m^2 s^{-1}
μ_{air}	Dynamic viscosity of air	1.8×10^{-5} Pa s

Note: Grain size diameters were measured with a caliper, giving $d=0.62$ mm for poppy seeds. $d=0.45$ mm for cornmeal and $d=1.7-2.2$ mm for millet. The range is given because they are not spherical.

$w=115\ \mu$m, equal to the typical grain size diameter for the grit on the sandpaper. The remaining experiments on cornmeal, salt, and millet, we assume that the air flows down through the granular medium. We estimate the flow velocity $u=(dV/dt)(1/a_w)$ with area $a_w=\pi d_i^2/4$ computed with the block annulus' inside diameter. The computed air flow velocity u versus pressure p measurements are shown in Fig. 8. We measured the slopes S of each set of points by fitting lines to the data points, and these slopes (in units of cm s^{-1} Pa^{-1}) are listed in Table 2.

The geometry of flow for our annular block is similar to that described for the air flow under the mechanism described in Eq. (12). Figure 8 shows linear fits to the air flow velocity versus pressure measurements. The nearly linear behavior supports our approximation given in Eq. (12) for air flow through a permeable medium caused by a pressure peak on the surface. A linear dependence of the flow rate on pressure is consistent with a low Reynolds number regime where air viscosity and permeability of the substrate are important. The lines in Fig. 8 do not go through the origin, so we do see evidence of non-linearity in the flow velocity versus pressure relation (for extensions to Darcy's law for airflow through agricultural grains see Refs. [34,35]). However, a vertical mechanism

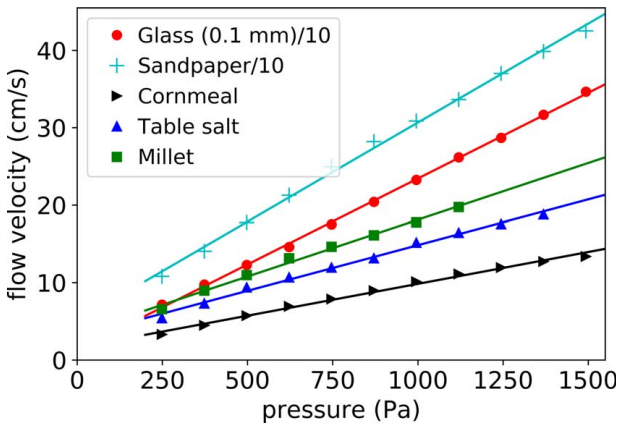

Fig. 8 Flow velocity versus pressure measurements for air forced under a flat annular block, while it was resting on a substrate. The points show measurements and lines show linear fits to the data. The slopes are listed in Table 2. We use these slopes to estimate the suction from air pressure on the mechanism. Because the velocities are higher on glass and sandpaper, these velocities (for both points and lines) have been divided by 10.

Table 2 Flow velocity versus pressure slopes

Substrate	Slope S
Glass plate, separation 0.1 mm	0.22
120 grit sandpaper	0.26
Cornmeal	0.0082
Common table salt	0.012
Millet	0.015

Note: Slopes S are given in cm s^{-1} Pa^{-1}. These are the slopes of the lines shown in Fig. 8. We estimate ±15% uncertainty in these measurements.

platform velocity $A\omega=40$ cm/s is well above the maximum measured flow velocity ~18 cm/s measured on the granular media. To apply the flow rate versus pressure measurements to our mechanism mechanics, we must extrapolate to larger values, rather than work in the low flow and nonlinear regime.

As was true in Sec. 3.1 for air flow under the mechanism, we assume that the air flow through a granular medium can be described by Darcy's law. The flow field below the substrate surface can again be approximated by Eqs. (11) and (12) but using the outer radius of the block annulus instead of the half-length of the mechanism as that is where the pressure must be equal to the atmospheric pressure. We take our experimentally measured pressure differential to be the central pressure p_0 in Eq. (11), and the measured air velocity to be the central velocity u_0 in Eq. (12). We expect the air flow velocity into the substrate inside the annulus

$$u \approx S\Delta p \tag{17}$$

where Δp is the air pressure differential and the slope S for air velocity versus pressure must be

$$S \approx \frac{\kappa}{\mu_{air}}\frac{2.4}{d_o/2} \tag{18}$$

following Eq. (13). Using the viscosity of air (listed in Table 1) and the slopes we measured on cornmeal, salt and millet (and listed in Table 2), Eq. (18) gives permeabilities of $\kappa=1-3\times10^{-7}$ cm^2. For loose sand, the permeability ranges from $\kappa\sim10^{-5}$ to 10^{-8} cm^2. Our measured slopes are consistent with permeability measurements in common porous media.

A comparison of Eqs. (17) and (18) with Eq. (12) implies that we can estimate the dimensionless coefficient α_z (Eq. (16)) with slopes S measured here and correcting for the ratio of the mechanism length and the block annulus' outer diameter, finding

$$\alpha_z = \frac{1}{2S}\frac{L}{d_o}\frac{L^2}{M\omega} = 2\left(\frac{0.015\ \text{cm s}^{-1}\ \text{Pa}^{-1}}{S}\right)\left(\frac{L}{4\ \text{cm}}\right)^3\left(\frac{1.4\ \text{g}}{M}\right) \tag{19}$$

$$\times\left(\frac{f}{12{,}000\ \text{rpm}}\right)\left(\frac{6\ \text{cm}}{d_o}\right) \tag{20}$$

The dimensionless parameter characterizing the suction $\alpha_z \gtrsim 1$, supporting our hypothesis that air pressure can affect the mechanism's dynamics. While we have described the force as a suction force, it would also operate to cushion the mechanism when it lands on the substrate.

3.3 Plane Poiseuille Flow. Plane Poiseuille flow describes steady laminar flow in a viscous fluid between two parallel sheets separated by a narrow distance z. Plane Poiseuille flow also obeys a relation between pressure gradient and flow velocity, similar to Darcy's law (Eq. (10)) and similar to our measured relation between flow velocity and pressure in Eq. (17). For Plane Poiseuille flow, a mean flow speed u (averaged over the velocity profile

between the plates) obeys

$$u = -\frac{z^2}{12\mu_{\text{air}}}\nabla p \tag{21}$$

Here, air flow is parallel to the plates as there is no flow through their surfaces. The similarity between Eq. (10) and Eq. (21), relating flow speed to a pressure gradient, implies that plane Poiseuille flow is consistent with an effective permeability $\kappa_{\text{PP}}(z) = z^2/12$ that depends on distance between the plates z.

We compare our flow velocity versus pressure measurements to the predictions of plane Poiseuille flow and then we will modify our estimate for the vertical drag force due to air pressure to take into account air motion parallel to the mechanism base when the mechanism is near but not on the granular substrate.

In Table 2 and with measurements shown in Fig. 8, we measured a flow velocity versus pressure for the annular block separated by 0.1 mm from a glass plate. We estimate the pressure gradient $\nabla p = 2\Delta p/(d_o - d_i)$ across the annulus. This presure gradient and Eq. (21) gives a predicted slope (describing pressure versus flow velocity) of $S = z^2/(12\mu_{air})2/(d_o - d_i)$. With $z = 0.1$ mm, this gives $S = 0.27\,\text{cm}\,\text{s}^{-1}\,\text{Pa}^{-1}$ and is consistent with the $0.22\,\text{cm}\,\text{s}^{-1}\,\text{Pa}^{-1}$ slope we measured. Our pressure versus flow rate measurement for the block near a glass plate are consistent with that estimated for plane Poiseuille flow.

Taking into account, viscous plane Poiseuille flow would give a height-dependent aerodynamic acceleration on our mechanism $a_{z,\text{aero}}(z)$. We use Eq. (7) to relate horizontal air speed u to vertical platform velocity v_z, Eq. (21) for Plane Poiseuille flow to estimate the pressure gradient under the mechanism as $\nabla p \sim 2p_0/L$ with p_0 under the platform and the force on the mechanism as $p_0 L^2$. This gives an estimate for the aerodynamic force on the mechanism due to air flow beneath the mechanism

$$F_{\text{PP,aero}} \sim -\frac{\mu_{\text{air}}}{z^2/12}\frac{L}{z}\frac{L^3}{8}v_z \tag{22}$$

This equation resembles the aerodynamic force we estimated from the permeability alone, Eq. (14), except the force becomes large as $z \to 0$. We expect the force cannot be higher than that estimated for the permeable medium. We can modify the acceleration of Eq. (15) to make a height-dependent transition to plane Poiseuille flow

$$a_{z,\text{aero}}(z) = -\alpha_z v_z \omega\left(\frac{1}{1 + (z/h_{PP})^3}\right) \tag{23}$$

and retaining the definition of the dimensionless parameter α_z of Eq. (16). The length that sets the transition between regimes

$$h_{PP} = (12L\kappa)^{\frac{1}{3}} = 0.17\,\text{mm}\left(\frac{L}{4\,\text{cm}}\right)^{\frac{1}{3}}\left(\frac{\kappa}{10^{-7}\text{cm}^2}\right)^{\frac{1}{3}} \tag{24}$$

and where we used our estimate for the permeability κ from Sec. 3.2 (see Eq. (18)). We define a dimensionless length $\bar{h}_{PP}$,

$$\bar{h}_{PP} = \frac{h_{PP}}{A} \approx 0.5\left(\frac{L}{4\,\text{cm}}\right)^{\frac{1}{3}}\left(\frac{\kappa}{10^{-7}\text{cm}^2}\right)^{\frac{1}{3}}\left(\frac{0.3\,\text{mm}}{A}\right) \tag{25}$$

4 Numerical Model for Locomotion

We describe the mechanism motion in two dimensions with x, z corresponding to horizontal and vertical coordinates. We use $\bar{x} = x/A$ and $\bar{z} = z/A$ for the coordinates in units of the vibration displacement amplitude A. Time τ is in units of ω^{-1} with $\tau = t\omega$. Velocity is in units of $A\omega$ and acceleration in units of $A\omega^2$. We assume that the mechanism base remains parallel to the granular substrate, with $\bar{z}$ giving the distance between substrate and mechanism base (in units of A) and $\bar{z} = 0$ for platform base touching a flat substrate. The center of the mechanism has $\bar{x} = 0$. We ignore tilting, rocking, flexing, and turning. Our additional nomenclature is listed in Table 3.

The equation of motions for our model resembles of that by Ref. [18] for harmonically driven micro-robots that either hop or move via stick-slip friction interactions, except here we also take into account the aerodynamic force discussed in Sec. 3. Our equation of motion for the mechanism's vertical coordinate $\bar{z}$ of the platform base center is

$$\frac{d^2\bar{z}}{d\tau^2} = -\Gamma^{-1} + \cos(\tau + \phi_0) + a_{z,\text{aero}} \tag{26}$$

where ϕ_0 is an initial phase for the motor. The recoil from the internal motion of the motor flywheel gives a sinusoidal acceleration of amplitude 1 in our dimensionless unit. The constant term, inversely dependent on the acceleration parameter, is due to gravity. The right-most term is from the force due to aerodynamics. The acceleration due to air pressure should only be significant when the mechanism is nearly touching the substrate. To reduce the aerodynamic acceleration as a function of height, we assume vertical acceleration

$$a_{z,\text{aero}} = -\frac{d\bar{z}}{d\tau}\alpha_z \exp(-\bar{z}/h_m) \tag{27}$$

The coefficient α_z is estimated in Sec. 3. Because the pressure should drop as the mechanism moves upward, we cut off the areodynamic force with a distance h_m that we treat as a free parameter. We expect $h_m \sim \bar{h}_{PP}$ estimated in Eq. (25) from the transition to plane Poiseuille flow. Because low Reynolds number flow is a poorer approximation at larger $\bar{z}$, we cut off the friction exponentially rather than with a power law (as in Eq. (23)). We have checked that the model gives similar trajectories with a $\bar{z}^{-3}$ rather than exponential cutoff in the drag force.

Our adopted equation of motion for the mechanism's horizontal coordinate $\bar{x}$ is similar to Eq. (26) but does not depend on gravity,

$$\frac{d^2\bar{x}}{d\tau^2} = \sin(\tau + \phi_0) + a_{x,\text{drag}} \tag{28}$$

with an additional height-dependent horizontal drag force $a_{x,\text{drag}}$.

We assume that the mechanism does not bounce off the substrate. When the trajectory reaches $\bar{z} = 0$, with vertical velocity $d\bar{z}/d\tau < 0$, and contacts the surface, we set the vertical velocity component to zero $d\bar{z}/d\tau = 0$. At the same time in the integration, we use a Coulomb friction law to set the horizontal component of acceleration due to contact with the surface. The frictional horizontal acceleration depends on the normal force exerted by the surface. With v_{x0}, v_{z0} equal to the velocity components prior to impact, we set the horizontal velocity after impact to be

$$\frac{d\bar{x}}{d\tau} = \begin{cases} v_{x0} - \text{sign}(v_{x0})\mu_s|v_{z0}| & \text{for } |v_{x0}| > \mu_s|v_{z0}| \\ 0 & \text{otherwise} \end{cases} \tag{29}$$

with μ_s the coefficient of friction which we set to the static value even though friction occurs when the mechanism is sliding on the substrate.

We allow a small horizontal drag force to be present, that is, in the same form as Eq. (27)

$$a_{x,\text{drag}}(\bar{z}) = -\alpha_x \frac{dx}{d\tau}\exp(-\bar{z}/h_m) \tag{30}$$

but with a different coefficient $\alpha_x < \alpha_z$. Our high-speed videos illustrate that grains are occasionally pushed and levitated as the mechanism moves. These interactions would slow the mechanism, acting like a horizontal drag force. Locomotion studies in granular media have previously adopted a hydrodynamic-like velocity-dependent drag force (e.g., Refs. [22,36]), though in these settings the locomotor is massive enough to penetrate into the medium. Even though the air pressure affects the vertical acceleration, shear in the air flow cannot exert a significant traction force horizontally. However if there is some contact with the surface when suction is strong, then the normal force on the mechanism could be higher

than computed using gravitational and motor recoil normal forces alone and this would enhance the horizontal friction force.

A challenge of numerically integrating a damped bouncing system is the "Zeno" effect, in which the number of bounces can be infinite in a finite length of time. Also because our forces depend on height, it is not straightforward to integrate from bounce to bounce, as commonly done for modeling a ball bouncing on a vibrating table top [29]. In our integrations, we take short time-steps and check for proximity to substrate $\bar{z} = 0$ each step. We update mechanism positions and velocities using straightforward first-order finite differences. We chose the time step to be sufficiently small that the trajectories are not dependent on it ($d\tau = 0.01$).

4.1 Model Mechanism Trajectories. Figure 9 shows a trajectory computed using Eqs. (26–30). Parameters for the model Γ, α_z, α_x, h_m, and μ_s are written in the top panel. Our dynamical system is similar to a vertically bouncing ball on a vibrating sheet (e.g., Refs. [29,31,37]). The bouncing ball can be described with a map between bounces, during which time the ball trajectory is specified by gravity alone [29]. Each bounce instantaneously changes the ball's vertical velocity, giving a condition that determines when the next bounce occurs. The dynamical system is rich, exhibiting period doubling and chaos [29,37]. The horizontal motion gives an additional degree of freedom that increases the complexity. For the bouncing ball above a vertically oscillating but parabolic plate, the vertical and horizontal motions are fully coupled; even a small curvature in the plate can induce the chaotic behavior [38]. Here, our x equation of motion depends on z but the z equation of motion does not depend on x.

In Fig. 9, the mechanism is begun above the substrate and initially is in free fall. While in free fall, the base of the mechanism oscillates due to the motor recoil. At $\tau \sim 5$, it contacts the surface, and its vertical velocity is reduced to zero. This happens each time it contacts the surface. Afterward touching the substrate, the velocity rises slowly because the acceleration must overcome the vertical drag force due to suction. The phase of oscillation is such that the horizontal velocity is near its minimum value when the motor is near the surface. Friction with the substrate and the horizontal drag force bring this minimum velocity toward zero. Because of the motor recoil, the mean horizontal velocity of the mechanism is above this minimum, and this gives the mechanism a net forward horizontal motion.

After integrating the equations of motion, the trajectory is resampled, so that the points are equally spaced with respect to time. In Fig. 9(*b*), the model trajectory is plotted with partially transparent points giving a lighter line where the velocity is slower. The model trajectory mimics the LED brightness traced in the photographs shown in Fig. 4. For the motor at 5.5 V and 285 Hz, the acceleration parameter is about 50 and the velocity of motion caused by recoil is about $A\omega = 52$ cm/s. The velocity of the mechanism we measured to be about 30 cm/s on poppy seeds, which is 0.57 in units of $A\omega$. We set $\alpha_z = 2$ with Eq. (20) consistent with $f = 285$ Hz, and using the slope of $S = 0.012$ cm s^{-1} Pa^{-1} measured on salt which has a similar grain size as poppy seeds. To match the vertical height exhibited by the trajectory, we adjusted h_m and we adjusted α_y to match the horizontal speed. We did not adjust the substrate coefficient of friction, setting it equal to the coefficient of static friction μ_s for our granular media. The value of $h_m = 0.4$, giving realistic-looking model trajectories, is consistent with that estimated for $\bar{h}_{PP}$, the height setting the transition between plane Poiseuille and permeable flow (see Eq. (25)). Our model is consistent with the heights reached by our observed mechanism trajectories and the strength of suction we estimated in Sec. 3 due to airflow below the mechanism base and through the substrate.

In Fig. 10, we show the effect of varying acceleration parameter, and in Fig. 11, the effect of varying the strength of the aerodynamic force. Coefficients for the models are printed on these figures. Period doubling is seen in Figs. 9(*b*), 10, and 11, similar to that seen in the photographs (Figs. 4 and 5). Some of the non-linear

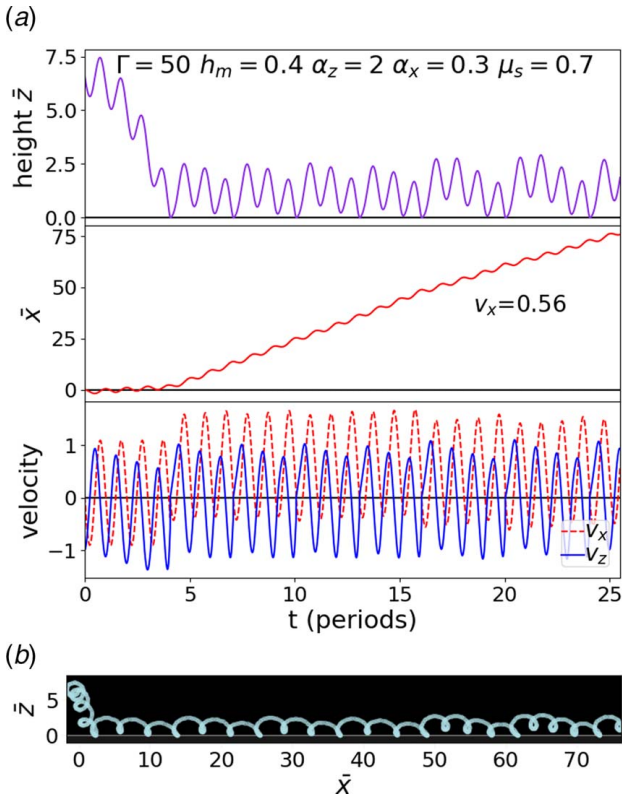

Fig. 9 (*a*) An integrated numerical model for mechanism locomotion. The top panel shows vertical motion or $\bar{z}(\tau)$, the middle panel shows horizontal motion or $\bar{x}(\tau)$. The bottom panel shows velocity components as a function of time. The trajectory is integrated for 25 motor oscillation periods using Eqs. (26) and (28). In the middle panel, the mean horizontal speed is labeled on the plot. The coefficients for the model are shown in the top panel with Γ the acceleration parameter, α_z and α_x setting the vertical and horizontal damping forces, the height h_m setting the cutoff height for them, and μ_s the coefficient of friction for the substrate. (*b*) The model mechanism trajectory $\bar{x}$ versus $\bar{z}$ is shown for the same numerical integration and can be compared with photographed trajectories in Figs. 4 and 5.

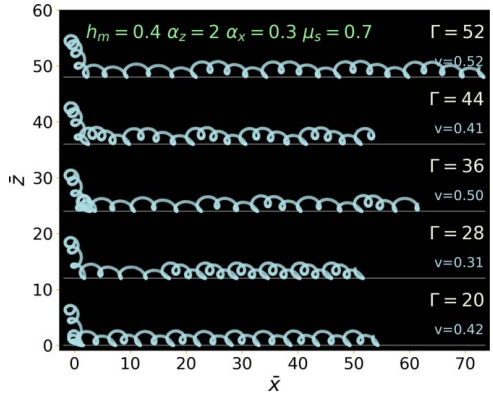

Fig. 10 Model mechanism trajectories for different acceleration parameters Γ. The higher acceleration parameter ones correspond to mechanisms with higher frequency motors. Average horizontal speeds are labeled for each trajectory on the right. Even though velocity in units of $A\omega$ is similar for these trajectories, the higher Γ models correspond to faster actual mean horizontal speeds as our unit of velocity is not independent of Γ.

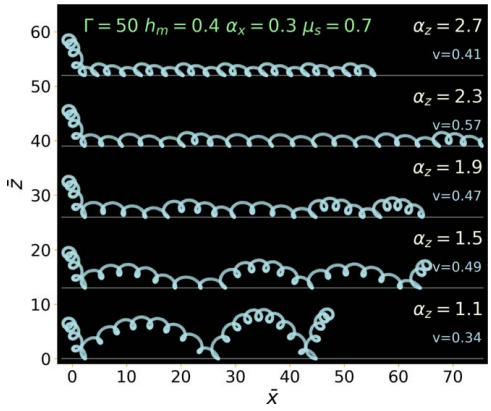

Fig. 11 Model mechanism trajectories for different damping parameters α_z. The fastest mechanism is second from top at $\alpha_z = 2.3$. This is faster because it gallops more efficiently, pushing off each period, instead of hopping into the air and pushing off the ground every few periods as is true of the lowest trajectory. The topmost trajectory is slower because the suction is so high; the mechanism does not launch itself off the ground for very long during each motor oscillation.

phenomena exhibited by the bouncing ball on the vibrating table top [37] is also exhibited by our vibrating mechanism model. By measuring the sensitivity to initial conditions and checking that exponential divergence of nearby trajectories is not dependent upon integration step size, we have verified that the model can exhibit chaotic behavior. However, our mechanisms traverse course media so irregularities in the measured trajectories are probably due to surface irregularities. As a consequence, we have not studied in detail the transition to chaos exhibited by this numerical model.

Figure 10 shows that trajectory speeds are not strongly dependent on the acceleration parameter. However, actual horizontal speeds at larger acceleration parameter Γ are likely to be higher than those at low Γ as the velocities are in units of $A\omega$. Mechanisms with larger vibrational amplitudes (larger recoil) and faster vibration would move horizontally at higher speeds.

While the model trajectories are not strongly dependent on acceleration parameter, they are, as seen in Fig. 11, dependent on the strength of the vertical drag force. We have noticed that mechanism motion is often jumpier on rougher substrates. The parameter $\alpha_z \propto S^{-1}$ (Eq. (20)) is smaller on rougher substrates, as we saw our pressure versus flow measurements S is larger for millet than salt or cornmeal. This is consistent with lower α_z models having trajectories that reach larger heights. Similar trajectories are observed without any horizontal damping force $\alpha_x = 0$, though the model is more chaotic, exhibiting speed variations and the mechanism sometimes changes direction entirely.

Horizontal speeds are labeled on each panel in Fig. 11 and show that the faster mechanism is the second from top with $\alpha_z = 2.3$. Also, the length of the trajectories in this figure is related to the average horizontal speed as each trajectory was integrated for the same time length of 25 motor periods. The fastest trajectory is fast because it gallops more efficiently, pushing off each motor oscillation period, instead of hopping into the air and pushing off the ground every few periods, as is true of other trajectories. The topmost trajectory is slower because the vertical drag is so high the mechanism does not launch itself effectively off the ground. This figure illustrates a speed optimization strategy for design. Mechanisms that are designed so that their center of mass does not make large vertical excursions during locomotion would be faster than those that propel the mechanism to larger heights, as during large vertical jumps the mechanism cannot push itself forward because it does not interact with the surface.

When the motor frequency is changed, both acceleration parameter and estimated parameter α_z vary, as α_z is inversely proportional to motor oscillation frequency (see Eq. (20)). At slower motor frequencies, the acceleration parameter Γ is lower and the vertical damping parameter α_z is higher. Figure 4 shows that at slower motor frequencies, the trajectories are more irregular, but this is opposite to that predicted by the model as higher α_z models tend to have flatter trajectories. The high-frequency trajectories on cornmeal, poppy seeds, and millet shown in Fig. 4 are similar; however, their permeabilities differ, and with different α_z, the modeled trajectories would have different shapes. We have noticed that the numerical model predicts similar trajectories for different α_z but at fixed α_z h_m and α_z/α_x, so the parameters describing our numerical model are not independent. Perhaps, the effective cutoff height parameter h_m should depend on the substrate. This is not unreasonable as finer-grained materials have higher α_z, and the high air pressure should primarily be important very close to the surface.

While our simple numerical model is successful at reproducing the shape and height of mechanism trajectories and the model is based on the size of the vertical drag force from flow versus pressure measurements, the description of the aerodynamic and friction forces needs improvement to be more predictive. Our model also neglects mechanism tilt, surface irregularities, flexing in the mechanism itself, and waves traveling along its power wires. An improved model could include these additional degrees of freedom.

Table 3 Additional nomenclature

Acceleration parameter	Γ
Pressure	p
Density	ρ
Permeability	κ
Bessel function	$J_0()$
Cylindrical coordinates	r, z
Time	t
Inside diameter	d_i
Outside diameter	d_o
Flow velocity versus pressure slope	S
Air flow rate	dV/dt
Air velocity	$\mathbf{u}$
Mechanism velocity	$\mathbf{v}$
Force	F
Acceleration	a
Initial motor phase	ϕ_0
Cartesian coordinates for model	$\bar{x}$, $\bar{z}$
Time coordinate for model	τ
Model parameters	α_z, α_x, h_m

5 Summary and Discussion

We have constructed a limbless, small (4 cm long), light-weight (less than 2 g), and low cost (a few dollars) mechanism, similar to a bristle bot, but with a coin vibrational motor on a light foam platform rather than bristles. The mechanism traverses granular media at speeds of up to 30 cm/s or 5 body lengths per second. In units of body lengths per second, our mechanism speed is similar to the six-legged DynaRoACH robot (10 cm long, 25 g) [25], but slower than the zebra-tailed lizard (10 cm long, 10 g) that can move 10 body lengths/s [24]. Our mechanism's horizontal speed exceeds many conventional bristle bots, it has no external moving parts, is lighter than most vibrational motor actuated bristle bots and can traverse flat granular media.

We estimate the mechanism's vibrational acceleration from the motor recoil divided by gravitation acceleration. Our mechanisms can have dimensionless acceleration parameters as large as 50. They would be classified as a hopper or galloper in terms of their gait or walking Froude number.

With an LED mounted to the mechanism and with long exposures, we photographed mechanism trajectories during locomotion. The mechanism trajectories are typically periodic, touching the granular substrate once per motor period, but sometimes they

show period doubling or tripling, where the mechanism touches the substrate once every two or three motor oscillation periods. The large dimensionless acceleration parameters imply that the trajectories should jump higher off the surface than they do when they are undergoing periodic motion. We infer that there must be a downward vertical force that keeps the mechanisms close to the surface. Following experimentation of mechanisms on different surfaces and with different bases, in vacuum and on granular media covered in powder, and with high-speed videos, we conclude that aerodynamics and substrate permeability to air affects their locomotion. Previous studies of locomotors traversing granular media did not require modeling of the aerodynamics and substrate permeability because the mechanisms were denser and heavier than ours or because locomotion was actuated by mechanism surfaces penetrating the granular substrate (e.g., see Sec. 5 in Ref. [21]).

Using experimental measurements of air flow rate versus pressure under blocks placed on different media, we estimated the size of a vertical aerodynamic force that is a suction force when the mechanism leaves the surface. The aerodynamics is modeled using Darcy's law for flow through permeable media and plane Poisseuille flow. In both settings, air flow velocity is proportional to air pressure gradient due to low Reynolds number flow in narrow spaces. When incorporated into a physical numerical model, the additional suction force lets us match mechanism trajectory heights, shapes, and speeds. The model is better behaved with a small additional horizontal drag force that might arise as some grains are disturbed and the power wires can transmit momentum. The physical model illustrates that horizontal mechanism speed is optimized by having large vibration amplitudes, large vibration frequencies, and a periodic trajectory that touches the surface once per oscillation period. Our mechanisms may be self-optimized if the mechanism platform flattens the substrate sufficiently to give effective suction as it traverses the medium. In the absence of air (for example on asteroid regolith) or lower atmospheric pressure (on Martian sand-dunes), a design could optimize speed by allowing the mechanism itself to flex. For example, a moving tail could act to limit the vertical motion and optimize speed this way, similar to the way the counter motion of a kangaroo's tail reduces the height a kangaroo reaches during each jump and minimizes the up and down motion of its center of mass.

The sensitivity of our kinematic model to air viscosity and substrate permeability suggests that construction and optimization of wider, lighter, or smaller mechanisms would depend on these parameters. Larger mechanisms that can traverse granular media with similar dynamics to our mechanisms might be constructed by designing the mechanism so that dimensionless parameter $\alpha_z \sim 1$, following Eq. (16). Despite their sensitivity to aerodynamics, we have found that the few gram hopper mechanisms we have constructed are fairly robust can traverse solid surfaces as well as a variety of granular medium, including sand, can traverse granular media in a vacuum, and they work when constructed from different types of light platform materials.

The mechanisms described here are not autonomous or maneuverable, though heavier types of bristlebots have been designed with these capabilities [39,40]. To achieve maneuverability, future studies could explore recoil vibrational motor based hoppers with dual vibrational motors or a single motor and an actuated way to vary its orientation. Additional capabilities would add weight to the mechanism and as hopper mechanism speeds depends on the mechanism recoil amplitude, this would reduce its speed. Lightweight motors are available with larger recoil, but they tend to be in cylindrical form with recoil motion vector traversing a cone or helix rather than coin form with recoil confined to plane as used here. The cylindrical motors would be more complex to model. To construct an energy-efficient locomotor, internal dissipation in the vibrational motor would have to be reduced. A BEAM-robotics style [41] autonomous locomotor might be achieved by constructing the mechanism platform from a light-weight solar panel. As vibrational motor-powered locomotion mechanisms can be inexpensive, autonomous BEAM-robotics style locomotors that are built with vibrational motors could in future be developed for multi-mechanism distributed exploration systems.

Acknowledgment

ACQ acknowledges support from the Simons Foundation 2017 and 2018. This material is based upon the work supported in part by the University of Rochester and National Science Foundation (Grant No. PHY-1460352). JKS gratefully acknowledges the support of ONR through Grant No. N00014-18-1-2456 (Program Manager Dr. Thomas Fu). We thank Scott Seidman, Michiko Feehan, Eric Nolting, and Mike Culver for their help in the laboratory.

References

[1] Childress, S., 1981, Mechanics of Swimming and Flying, Cambridge Studies in Mathematical Biology, Cambridge University Press, Cambridge, UK.
[2] Hirose, S., 1993, *Biologically Inspired Robots: Snake-Like Locomotors and Manipulators*, Oxford University Press, Oxford, UK.
[3] Alexander, R. M., 2003, *Principles of Animal Locomotion*, Princeton University Press, Princeton, NJ.
[4] Guo, Z. V., and Mahadevan, L., 2008, "Limbless Undulatory Propulsion on Land," Proc. Natl. Acad. Sci., **105**(9), pp. 3179–3184.
[5] Childress, S., Hosoi, A., Schultz, W. W., and Wang, J., 2012, eds., Natural Locomotion in Fluids and on Surfaces: Swimming, Flying, and Sliding, The IMA Volumes in Mathematics and Its Applications, Vol. 155, Springer, New York.
[6] Chernous'ko, F. L., and Shunderyuk, M. M., 2010, "The Influence of Friction Forces on the Dynamics of a Two-Link Mobile Robot," J. Appl. Math. Mech., **74**(1), pp. 13–23.
[7] Noselli, G., and DeSimone, A., 2014, "A Robotic Crawler Exploiting Directional Interactions: Experiments, Numerics and Derivation of a Reduced Model," Proc. Roy. Soc. A, **470**(2171), p. 20140333.
[8] Wagner, G. L., and Lauga, E., 2013, "Crawling Scallop: Friction-Based Locomotion With One Degree of Freedom," J. Theor. Biol., **324**(7), pp. 42–51.
[9] Giomi, L., Hawley-Weld, N., and Mahadevan, L., 2013, "Swarming, Swirling and Stasis in Sequestered Bristle-Bots," Proc. R. Soc. A, **469**(2151), p. 20120637.
[10] Hosoi, A. E., and Goldman, D. I., 2015, "Beneath Our Feet: Strategies for Locomotion in Granular Media," Annual Rev. Fluid Mech., **47**(1), pp. 431–453.
[11] Maladen, R. D., Ding, Y., Umbanhowar, P. B., and Goldman, D. I., 2011, "Undulatory Swimming in Sand: Experimental and Simulation Studies of a Robotic Sandfish," Int. J. Robot. Res., **30**(7), pp. 793–805.
[12] Hatton, R. L., Burton, L. J., Hosoi, A., and Choset, H., 2011, "Geometric Maneuverability With Applications to Low Reynolds Number Swimming," Proceedings of the 2011 IEEE/RSJ International Conference on Intelligent Robots and Systems (IROS), Sept. 25–30, IEEE, New York, pp. 3893–3898.
[13] Cicconofri, G., and DeSimone, A., 2015, "Motility of a Model Bristle-Bot: A Theoretical Analysis," Inter. J. Non-Linear Mech., **76**(Nov.), pp. 233–239.
[14] Scholz, C., D'Silva, S., and Poeschel, T., 2016, "Ratcheting and Tumbling Motion of Vibrots," New. J. Phys., **18**(12), p. 123001.
[15] DeSimone, A., and Tatone, A., 2012, "Crawling Motility Through the Analysis of Model Locomotors: Two Case Studies," European Phys. J. E, **35**(9), p. 85.
[16] Oskay, W., 2007, "Bristlebot: A Tiny Directional Vibrobot", http://www.evilmadscientist.com/2007/bristlebot-a-tiny-directional-vibrobot/.
[17] Chatterjee, S., Chatterjee, S., and Singha, T. K., 2005, "On the Generation of Steady Motion Using Fast-Vibration," J. Sound Vib., **283**(3–5), pp. 1187–1204.
[18] Jalili, H., Vossoughi, G., and Salarieh, H., 2016, "Motion Analysis of a Vibrational Micro-Robot With Two Perpendicular Harmonic Actuators and Deriving the Design Parameters in Stick-slip-Jump Mode," J. Sound. Vib., **372**(June), pp. 266–282.
[19] Majewski, T., Szwedowicz, D., and Majewski, M., 2017, "Locomotion of a Mini Bristle Robot With Inertial Excitation," J. Mech. Robot., **9**(6), p. 061008.
[20] Tsimring, L., and Volfson, D., 2005, "Modeling of Impact Cratering in Granular Media," Proceedings of the International Conference on Powders & Grains, Stuttgart, Germany, July 18–22, R. Garcia-Rojo, H. J. Herrmann, and S. McNamara, eds., A.A. Balkema Publishers, Leiden, The Netherlands, vol. 2, pp. 1215–1222.
[21] Aguilar, J., Zhang, T., Qian, F., Kingsbury, M., McInroe, B., Mazouchova, N., Li, C., Maladen, R., Gong, C., Travers, M., Hatton, R. L., Choset, H., Umbanhowar, P. B., and Goldman, D. I., 2016, "A Review on Locomotion Robophysics: The Study of Movement At the Intersection of Robotics, Soft Matter and Dynamical Systems," Rep. Prog. Phys., **79**(11), p. 110001.
[22] Aguilar, J., and Goldman, D. I., 2016, "Robophysical Study of Jumping Dynamics on Granular Media," Nat. Phys., **12**(3), pp. 278–283.
[23] Knight, J. B., Jaeger, H. M., and Nagel, S., 1993, "Vibration-Induced Size Separation in Granular Media: The Convection Connection," Phys. Rev. Lett., **70**(24), p. 3728–3731.
[24] Li, C., Hsieh, S. T., and Goldman, D. I., 2012, "Multi-functional Foot Use During Running in the Zebra-Tailed Lizard (callisaurus Draconoides)," J. Exp. Biol., **215**(18), pp. 3293–3308.
[25] Zhang, T., Qian, F., Li, C., Masarati, P., Hoover, A. M., Birkmeyer, P., Pullin, A., Fearing, R. S., and Goldman, D. I., 2013, "Ground Fluidization Promotes Rapid Running of a Lightweight Robot," Int. J. Robot. Res., **32**(7), pp. 859–869.

[26] Childress, S., Spagnolie, S. E., and Tokieda, T., 2011, "A Bug on a Raft: Recoil Locomotion in a Viscous Fluid," J. Fluid. Mech., **669**(Feb.), pp. 527–556.
[27] Bagnold, R. A., 1954, "Experiments on a Gravity-Free Dispersion of Large Solid Spheres in a Newtonian Fluid Under Shear," Proc. Roy. Soc. A, **225**(1160), pp. 49–63.
[28] Alexander, R. M., 1984, "The Gaits of Bipedal and Quadrupedal Animals," Int. J. Robot. Res., **3**(2), pp. 49–59.
[29] Holmes, P. J., 1982, "The Dynamics of Repeated Impacts With a Sinusoidally Vibrating Table," J. Sound Vib., **84**(2), pp. 173–189.
[30] Bapat, C. N., Sankar, S., and Popplewell, N., 1986, "Repeated Impacts on a Sinusoidally Vibrating Table Reappraised," J. Sound Vib., **108**(1), pp. 99–115.
[31] Germinard, J. C., and Laroche, C., 2003, "Energy of a Single Bead Bouncing on a Vibrating Plate: Experiments and Numerical Simulations," Phys. Rev. E, **68**(3), p. 031305.
[32] Chastaing, J.-Y., Bertin, E., and Geminard, J.-C., 2015, "Dynamics of the Bouncing Ball," Am. J. Phys., **83**(Jan.), p. 518.
[33] Alexander, R. M., and Jayes, A. S., 1983, "A Dynamic Similarity Hypothesis for the Gaits of Quadrupedal Mammals," J. Zool. (London), **201**(1), pp. 135–152.
[34] Ergun, S., 1952, "Fluid Flow Through Packed Columns," Chem. Eng. Prog., **48** (2), pp. 89–94.
[35] Molenda, M., Montross, M. D., McNeill, S. G., and Horabik, J., 2005, "Airflow Resistance of Seeds At Different Bulk Densities Using Ergun's Equation," Trans. Am. Soc. Agri. Eng., **48**(3), pp. 1137–1145.
[36] Katsuragi, H., and Durian, D. J., 2013, "Drag Force Scaling for Penetration Into Granular Media," Phys. Rev. E, **87**(5), p. 052208.
[37] Pieranski, P., 1983, "Jumping Particle Model. Period Doubling Cascade in An Experimental System," J. Phys., **44**(5), pp. 573–578.
[38] McBennett, B. G., and Harrisa, D. M., 2016, "Horizontal Stability of a Bouncing Ball," Chaos, **26**(9), p. 093105.
[39] Vartholomeos, P., and Papadopoulos, E., 2006, "Dynamics, Design and Simulation of a Novel Microrobotic Platform Employing Vibration Microactuators," Trans. ASME, **128**(1), pp. 122–133.
[40] Vlachos, K., Papadimitriou, D., and Papadopoulos, E., 2015, "Vibration-Driven Microrobot Positioning Methodologies for Nonholonomic Constraint Compensation," Engineering, **1**(1), pp. 66–72.
[41] Smit, M. C., and Tilden, M., 1991, "BEAM Robotics," Algorithm, **2**(2), pp. 15–19.